2017 IEEE Conference on Control Technology and Applications (CCTA)
August 27-30, 2017. Kohala Coast, Hawai'i, USA

Modeling and Control of a Cable Driven Modular Snake Robot

Peter Racioppo
Robotics and Mechatronics Lab
Department of Mechanical Engineering
Virginia Tech
Blacksburg, VA, USA
rpeter8@vt.edu

Pinhas Ben-Tzvi
Robotics and Mechatronics Lab
Department of Mechanical Engineering
Virginia Tech
Blacksburg, VA, USA
bentzvi@vt.edu

Abstract—**This paper presents the modeling and control of a planar snake robot composed of modular, single degree of freedom bending units. The goal of this research is to design a snake robot that minimizes the number of degrees of freedom necessary for planar serpentine locomotion, while closely approximating the idealized sinusoidal shape of a moving snake. The use of an underactuated, multi-link module as the snake's basic functional unit aims at simplifying the control of snake robots while retaining the advantages of highly articulated designs. The design and dynamic model of the snake robot are presented, and a controller is developed that demonstrates path following between waypoints and disturbance rejection, under viscous and Coulomb frictional models. Controller design for the reduced-DOF snake is presented and related to the control of snake robots that independently actuate all of their joints. Key control and design parameters are then optimized to produce curvature profiles that maximize the robot's forward speed.**

Keywords—snake robotics; underactuation; cable-actuation; serpentine locomotion

I. Introduction

Snake robots have been the subject of much research in the robotics community due to the advantages of their body structure and locomotion style in irregular environments. Like their biological counterparts, snake robots are composed of a series of discrete links and move with sinusoidal "serpentine" motions that produce propulsive frictional forces.

Shigeo Hirose [1] is widely credited with pioneering the field of snake robotics with his development of ACM III, the first snake robot, and his discovery of the "serpenoid curve," an approximation for the shape of a biological snake performing serpentine motion. Further work on mathematical descriptions of serpentine locomotion was conducted by Shugen Ma [2], who compared the locomotive efficiency of various curvature profiles and developed an alternative to the serpenoid curve. Other approaches to achieving planar locomotion include Chernousko's study of a 3-link snake robot, in which the joint angles are made to perform "elementary motions" from which more complex gaits can be built [3]. Liljebäck et al. demonstrated a path following control scheme and waypoint guidance in a snake robot approximating the serpenoid curve, both in simulation and experimentally [4]–[5]. Liljebäck et al. also proved that anisotropic ground friction is a necessary condition for controllable locomotion, developed a simplified model of serpentine locomotion consisting of only translational motions, and tested jamming resolution schemes during interaction with obstacles [6]–[7]. Optimization of snake robot design parameters has also been a major focus of research, particularly with the aim of maximizing the robot's average speed [3],[8].

The majority of previous work on snake robots has focused on snakes in which each of the joint angles is actuated independently [9]–[12], which we refer to here as "full-degree of freedom (DOF)" snakes. This paper explores the use of a single-DOF, cable-driven bending mechanism in place of an individually actuated rigid link as the basic functional unit of a "reduced-DOF" snake robot. This design approach aims to maximize the locomotive efficiency of serpentine locomotion achievable per degree of freedom, simplify control, and decrease mass and cross-sectional area requirements. This paper is part of ongoing work on the use of cable-actuated serpentine mechanisms, for use in robotic tails and snakes [13]–[21] and is organized as follows: Section II presents the design of the bender mechanism. Section III presents a multibody dynamic model, accounting for the effects of cable actuation. Section IV introduces past work on snake locomotion and develops feedforward and integral controllers based on the dynamic model. Section V discusses modifications to the control scheme to account for reduced-DOF snakes and unequal link lengths and explores optimal design and control parameters. Plans for future work are discussed in Section VI.

II. Design

This section presents the design of the planar bender mechanism. Each bender is a single-DOF unit consisting of a serial linkage of rigid segments connected by revolute joints. The mechanism is actuated by one antagonistic cable pair per link, each of which is routed around the circular surfaces of the links below it and terminates on a multi-radius pulley, whose radii determine the bender's curvature profile. Rotation of the pulley results in a planar bending motion. Circular routing ensures approximately equal and opposite displacements in antagonistic cable pairs. Extension springs placed in series with the cables add

compliance to the mechanism, allowing for passive conformation to obstacles.

Fig. 1(A) shows the design of a 6-link bender that uses passive wheels to produce the anisotropic frictional characteristics required for locomotion. A snake robot may be built from multiple benders by connecting them in series using a male-female interface, with two benders the minimum required for planar locomotion and turning. Locomotion may be achieved by oscillating each bender sinusoidally. Turning occurs when the maximum angular displacements on the left and rights sides of the benders are unequal, resulting in an average torque that rotates the robot.

III. Dynamic Model

This section presents a multibody dynamic (MBD) model of a snake robot and a brief treatment of cable actuation in this context. The advantage of an MBD approach is that it removes the need for the idealized no side-slip constraints commonly employed in previous models, and clearly partitions forces internal to the mechanism into a vector of Lagrange multipliers.

The snake robot is modeled as N straight, rigid links, connected in series by revolute joints, where link i is of half-length L_i, mass m_i, and moment of inertia I_i. The positions of the N link centers in the xy-plane are specified by a vector of generalized coordinates $\mathbf{q} = [\mathbf{q}_1,\ldots,\mathbf{q}_N]^{\mathrm{T}}$ where $\mathbf{q}_i = [\mathbf{r}_i,\ \phi_i]^{\mathrm{T}}$ gives the global position $\mathbf{r}_i = [x_i,\ y_i]^{\mathrm{T}}$ and orientation ϕ_i of the ith link, with respect to a fixed, global frame at the origin, as shown in Fig. 1(B). Each revolute joint is defined by two algebraic constraint equations, which are assembled into the vector equation $\mathbf{\Phi}(\mathbf{q},t) = 0$, of length $N_c = 2(N-1)$.

The rotation matrix $\mathbf{R}_i$, corresponding to a rotation about the z-axis by an angle ϕ_i, transforms the global position $\boldsymbol{r}_i$ of a link from the global frame to the ith link frame. The local x and y coordinates are taken to be normal to the link and along the link, respectively. The anisotropic frictional characteristics of the snake are modeled by defining normal and transverse coefficients of friction c_n and c_t, which act along the local x and y directions, respectively. The external frictional force produced by the motion of the ith link's center of mass (CM) directly depends on the global velocity vector $\dot{\mathbf{r}}_i$.

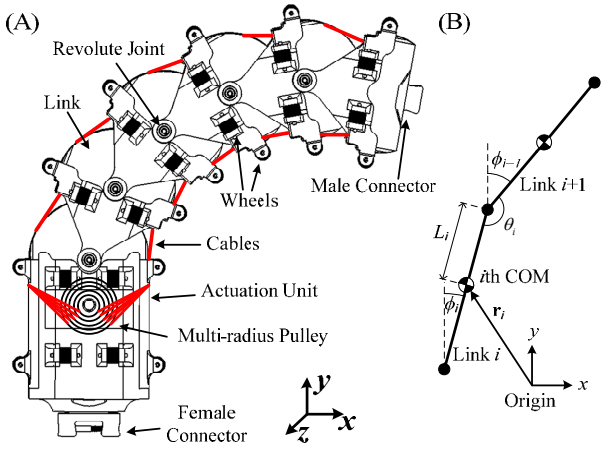

Fig. 1. (A) Design of a 6-link bender; (B) Coordinate definitions

The friction force $\mathbf{F}_{f,i}(\dot{\mathbf{r}}_i,\phi_i)$ acting on link i is determined by rotating $\dot{\mathbf{r}}_i$ into the local frame, to account for the locally defined frictional characteristics, and then rotating the local force back into the global frame. A viscous force on the CM of the ith link is thus given by

$$\mathbf{F}_{f,i}(\dot{\mathbf{r}}_i,\phi_i) = -\mathbf{R}_i\mathbf{\Omega}_i\mathbf{R}_i^{\mathrm{T}}\dot{\mathbf{r}}_i \tag{1}$$

where $\mathbf{\Omega}_i = \mathrm{diag}(c_{n,i}, c_{t,i})$ is a diagonal matrix of the normal and transverse coefficients of friction, respectively. Alternatively, a Coulomb frictional force acting on the ith link's CM may be defined by

$$\mathbf{F}_{f,i}(\dot{\mathbf{r}}_i,\phi_i) = -m_i g\mathbf{R}_i\mathbf{\Omega}_i\mathbf{sgn}(\mathbf{R}_i^{\mathrm{T}}\dot{\mathbf{r}}_i) \tag{2}$$

where g is gravitational acceleration and **sgn** is a vector operator which performs the signum function on each element of its argument. For simplicity, all simulations in this paper assume viscous friction.

The frictional forces due to translation of a link and pure rotation of the link about its CM must be accounted for separately. To account for the frictional torque produced by a pure rotation, each half-link is treated as consisting of n equal masses, separated by a length $l_{n,i} = 2L_i/(2n+1)$. For a link of orientation ϕ_i and angular velocity $\dot{\phi}_i$, the x and y velocities of the nth segment due to a pure rotation of the link are $v_{x,n} = \dot{\phi}_i l_{n,i}\cos\phi_i$ and $v_{y,n} = -\dot{\phi}_i l_{n,i}\sin\phi_i$, respectively. The frictional forces on each segment may then be calculated using (1) or (2). Since the frictional forces on the nth segment are linear with $l_{n,i}$, the forces produced by the n segments are equivalent to a force on a single mass, located at an effective length along the link of

$$l_{\mathrm{eff},i} = l_{n,i}\sum_{n'=0}^{n}\frac{n'}{n} = \frac{n+1}{2n+1} \tag{3}$$

and in the limit that n goes to infinity, $l_{\mathrm{eff},i} = ½$. Defining $\mathbf{v}_i = \dot{\phi}_i l_{\mathrm{eff},i}\left[\cos\phi_i \quad \sin\phi_i\right]^{\mathrm{T}}$, the frictional torque acting on link i may be written, with reference to (1) and (2), as

$$\tau_{\mathrm{f},i} = l_{\mathrm{eff},i}\mathbf{F}_{\mathrm{f},i}(\mathbf{v}_i,\phi_i) \tag{4}$$

The torque produced at each of the joints by the action of the cables may be calculated by observing that all of the cable tensions acting on joint i occur in equal and opposite pairs, except those acting between links i–1 and i. The relation between motor torque and joint torque is thus given in terms of the ith link radius R_i and cable tension T_i by the system of equations

$$\tau_{\mathrm{M}} = \sum_{i=1}^{N} F_i r_i \quad , \quad \tau_i = \sum_{j=i}^{N} F_j l_j \tag{5}$$

where τ_M is the torque applied by the motor and r_j is the jth pulley radius [21]. Springs of spring constant k_i are attached in series with each of the cables, producing a cable tension on the ith segment of $T_i = -k_i r_i \theta_P$, where r_i is the ith pulley section and θ_P is the pulley's angular displacement. The approximate angular displacement θ_i at each joint due to a pulley rotation of θ_P is given by the relation

$$\theta_i = \alpha_i \theta_P \tag{6}$$

where $\alpha_i = (r_i/D_i - r_{i-1}/D_{i-1})$ and $D_i \approx (L_i^2 + R_i^2)^{1/2}$ [21]. The torque applied on joint i by the springs is $\tau_i = -\kappa_i \theta_i$ where

$$\kappa_i = \alpha_i \sum_{i=j}^{N-1} \frac{k_j r_j R_j}{\alpha_j^2} \tag{7}$$

Choosing the ith spring constant according to (7) so that $\kappa_i = \kappa_j$ for all $i, j \in \{1, \ldots, N-1\}$, the effect of the linear springs may be treated as equivalent to that produced by equally valued torsional elements located at each joint. Positive spring constants obeying this condition may always be found, provided that α_i increases monotonically with increasing i.

The forces acting on each link are assembled into the generalized force vector $\mathbf{Q}^A$. Defining a mass matrix $\mathbf{M} = \text{diag}(m_i, m_i, I_i, \ldots, m_N, m_N, I_N)$, the $3N+N_c$ constrained variational equations of motion may then be written as

$$\delta \mathbf{q}^T \left[\mathbf{M}\ddot{\mathbf{q}} - \mathbf{Q}^A \right] = 0 \tag{8}$$

where $\delta\mathbf{q}$ is an infinitesimal displacement in the generalized coordinate vector $\mathbf{q}$, consistent with $\mathbf{\Phi}(\mathbf{q}, t) = 0$ [22]. Introducing a vector $\boldsymbol{\lambda}$ of Lagrange multipliers, the system may be reformulated as a matrix differential algebraic equation of motion (DAE)

$$\begin{bmatrix} \mathbf{M} & \mathbf{\Phi}_\mathbf{q}^T & \mathbf{0} \\ \mathbf{\Phi}_\mathbf{q} & \mathbf{0} & \mathbf{0} \\ \mathbf{0} & \mathbf{0} & \mathbf{I} \end{bmatrix} \begin{bmatrix} \ddot{\mathbf{q}} \\ \boldsymbol{\lambda} \\ \dot{\mathbf{q}} \end{bmatrix} = \begin{bmatrix} \mathbf{Q}^A \\ \boldsymbol{\gamma} \\ \dot{\mathbf{q}} \end{bmatrix} \tag{9}$$

where $\mathbf{\Phi}_\mathbf{q}$ is the Jacobian and $\boldsymbol{\gamma}$ is a vector of acceleration independent terms [23]. Initial velocities must be consistent with the constraint $\mathbf{\Phi}_\mathbf{q}\dot{\mathbf{q}} = -\mathbf{\Phi}_t$, where $\mathbf{\Phi}_t$ is the time derivative of the constraint vector $\mathbf{\Phi}$. Inverting the left-hand-side matrix in (9), the state vector $\mathbf{Y} = \begin{bmatrix} \ddot{\mathbf{q}} & \boldsymbol{\lambda} & \dot{\mathbf{q}} \end{bmatrix}^T$ may be found with the use of a numerical DAE solver.

IV. Full-DOF Snake

This section reviews previous formulations of the serpentine gait and necessary conditions for forward locomotion. A controller for an N-link, full-DOF snake robot performing this gait is then introduced.

A. Serpentine Locomotion

An N-link snake robot may approximate the shape of a biological snake undergoing serpentine motion by driving its $N-1$ joint angles $\theta_i = \phi_{i+1} - \phi_i$ to track the reference angle

$$\theta_{\text{ref},i} = \alpha \sin\left(\omega t + (i-1)\delta\right) + \theta_0 \tag{10}$$

where α is the joints' maximum angular displacement, ω is the angular velocity, δ is a phase-offset between links, and θ_0 is an offset which induces turning for nonzero values [8]. Following the approach in Liljebäck et al. [24], a PD controller on the ith joint angle may be written as

$$\bar{U}_i = P\left(\theta_{\text{ref},i} - \theta_i\right) + D\left(\dot{\theta}_{\text{ref},i} - \dot{\theta}_i\right) \tag{11}$$

where $\theta_{\text{ref},i}$ is set according to (10), and P and D are constant proportional and derivative gains. In a simplified model of a snake robot given by [8], the phase-offset δ that maximizes the robot's forward speed may be approximated as

$$\delta_{\text{opt}} = \frac{\pi}{N-1} \tag{12}$$

B. Feedforward Control

Defining a vector of link orientations $\boldsymbol{\phi} = [\phi_1, \ldots, \phi_N]^T$, the system's equations of motion are comprised of one equation per generalized coordinate of the form:

$$f_i(\ddot{\mathbf{r}}_i) + g_i(\boldsymbol{\lambda}) = F_{\text{ext},i} \tag{13}$$

and one equation per revolute constraint of the form:

$$h_i(\ddot{\mathbf{r}}) + j_i(\boldsymbol{\phi}, \ddot{\boldsymbol{\phi}}) = k_i(\boldsymbol{\phi}, \dot{\boldsymbol{\phi}}) \tag{14}$$

for some functions f_i, g_i, h_i, j_i, and k_i, and the generalized external force $F_{\text{ext},i}$. For x and y coordinates, $F_{\text{ext},i}$ consists solely of frictional forces, but for angular coordinates ϕ_i, it includes an actuation torque U_i. Thus, a $U_i = U_{i,\text{lin}} + \bar{U}_i$ may be chosen so that $U_{i,\text{lin}}$ cancels $g_i(\boldsymbol{\lambda})$ and undesirable external forces. The angular acceleration of joint i is then proportional to the desired input $\bar{U}_i$, which tracks the serpenoid curve according to (11). The linearizing feedforward input $U_{i,\text{lin}}$ is a function of $\boldsymbol{\lambda}$. Solving the $3N$ equations of (13) for the $3N$ elements of $\boldsymbol{\lambda}$, $U_{i,\text{lin}}$ may finally be written as a function of the generalized coordinates and their derivatives.

C. Path Following Control

A snake robot driving its joint angles according to (10) moves in a straight line for $\theta_0 = 0$ and at constant radius of curvature for constant, nonzero θ_0 [24]. In Liljebäck et al. [4], a path following controller is defined by setting

$$\theta_0 = A_h \left(h - h_{\text{ref}}\right) \tag{15}$$

where the heading $h = \frac{1}{N-1}\sum_{i=1}^{N}\theta_i$ is the average joint angle, A_h is a constant gain, and h_{ref} is the desired heading, defined as

$$h_{\text{ref}} = -\arctan(P_{\text{X}} / \Delta) \tag{16}$$

where the "cross track error" P_{X} is the shortest distance from the snake's CM to the desired path and Δ is the constant "look-ahead distance."

Alternatively, the cross track error for the ith link and jth waypoint may be defined as

$$p_{\text{x},ij} = \sqrt{\left| K_{i,j-1}{}^2 - \left(2E_j\right)^{-2}\left(K_{i,j-1}{}^2 - K_{i,j}{}^2 + E_j{}^2\right)^2 \right|} \tag{17}$$

where $K_{i,j}$ is the distance from the ith link frame to the jth waypoint and E_j is the distance between the $(j-1)$th and jth waypoints. A single cross track error $p_{\text{x},j}$ may then be defined as a weighted average over the links. Defining $\mathbf{v}_{ij} = [v_{ij,x}\ v_{ij,y}]^{\text{T}}$ as the vector from the ith link frame to the current waypoint and $\mathbf{w}_j = [w_{j,x}\ w_{j,y}]^{\text{T}}$ as the vector between the current waypoint and the previous waypoint, a signed cross track error may be defined as $P_{\text{X},j} = -\text{sgn}(\theta_{\text{rel}} - \theta_{\text{wp}})p_{\text{x},j}$, where

$$\theta_{\text{rel}} = \arctan\left(\frac{v_{ij,x}}{v_{ij,y}}\right), \quad \theta_{\text{wp}} = \arctan\left(\frac{w_{j,x}}{w_{j,y}}\right) \tag{18}$$

Here, the signum function determines which side of the desired path the robot is on. The angle between desired paths θ_{wp} is also used to ensure that when switching paths the robot always turns through the smaller angle between paths. In place of (16), the desired heading for the jth waypoint is set according to

$$h_{\text{ref}} = -\arctan\left(P_h P_{\text{X},j} + I_h \int_0^t P_{\text{X},j}\,dt' + D_h \dot{P}_{\text{X},j}\right) + \theta_{\text{wp}} \tag{19}$$

The integral term in (19) acts to compensate for steady state error in the distance of the snake robot from the desired path, under large disturbance forces due, for example, to obstacles, water currents, or gravitational forces. Special care must be taken to avoid instabilities in the integral term under large errors, and in particular during the transient states when the snake is switching targets. Thus, if either the cross track error P_{X} or the heading error $|\theta_{\text{rel}} - \theta_{\text{wp}}|$ pass some maximum values, the integral term is reset to zero. The heading gains must also obey the condition $I_h/P_h < H$ for a constant H, to prevent the snake from banking too hard.

Fig. 2 displays a comparison of path-following errors with and without the integral term, for a 3-link, full-DOF snake following the line $x = 0$, under a constant disturbance in the positive x-direction. The link length L_i is taken to be a constant L for all i, and the position of the robot's "head" (the end of its first link) is plotted in units of L.

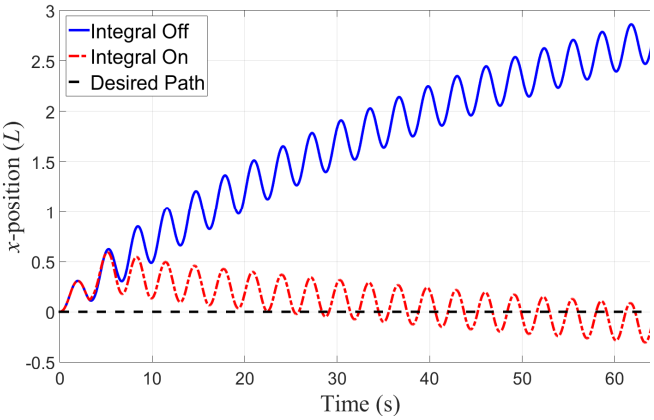

Fig. 2. Path following under a disturbance

V. Reduced-DOF Snake

Two degrees of freedom are sufficient for a snake robot to perform planar serpentine locomotion, but a snake with only three rigid links can only form a sawtooth approximation to the serpenoid curve. An improved fit to the serpenoid curve may be achieved without increasing the number of degrees of freedom by substituting coupled bending mechanisms in place of each pair of rigid links. This section presents modifications to the modeling and control presented in Sections III and IV to account for a reduced-DOF snake robot, as well as optimizations of control and design parameters.

A. Control

A model of a reduced-DOF snake robot composed of bender mechanisms may be obtained from the model in Sec. III by concatenating $N-2$ constraints to the constraint vector $\mathbf{\Phi}(\mathbf{q},t)$, according to the joint angle relation given by (6). If L_i is constant for all $i \in \{1,\ldots,N\}$, (6) reduces to

$$\frac{r_N}{r_1} = \frac{1}{\theta_1}\sum_{i=1}^{N}\theta_i \tag{20}$$

By analogy with (11), locomotion is achieved by applying a controller on the sum of each bending unit's joint angles. By proper selection of the pulley radius ratios r_i/r_1, the kth bender may be made to individually approximate a half-period of a sinusoid by applying a motor torque of

$$\bar{U}_k = P\left(\theta_{\text{ref}} - \sum_{i=1}^{N-1}\theta_{k,i}\right) + D\left(\dot{\theta}_{\text{ref}} - \sum_{i=1}^{N-1}\dot{\theta}_{k,i}\right) \tag{21}$$

where N is the number of links in each bender, P and D are constant gains, $\theta_{k,i}$ is the ith joint angle of the kth bender, and θ_{ref} is again given by (10). The torques acting on each joint as a result of (21) may be calculated using (5), and then fed directly into the feedforward law described in Sec. III.B.

Alternately, we can apply a controller on the lateral displacement of each bender's sinusoidal motion, given for an N-link bender by

$$A \approx \sum_{i=1}^{m} 2L_i \sin(\psi_i) \tag{22}$$

where ψ_i is defined, in terms of the joint angles θ_i, as

$$\psi_i = \begin{cases} \left(\sum_{j=i}^{m} \theta_j - \frac{\theta_m}{2} \right), & \text{even } N \\ \sum_{j=i}^{m} \theta_j, & \text{odd } N \end{cases} \tag{23}$$

where $m = \text{floor}(N/2)$. By (22), a snake robot obeying (10) with $\delta \approx \delta_{\text{opt}}$ has a lateral displacement of the form

$$A_{\text{ref}} \approx \frac{S}{m} \sum_{i=1}^{m} \sin\left(c_1 \sin\left(\tfrac{\pi}{2m}(i-1)c_2 \right) + \tfrac{\pi}{2m}(i-1)c_3 \right) \tag{24}$$

where S is the sum of the link lengths and c_1, c_2, and c_3 are control variables. Thus, a PD "Lateral Motion Controller" for a reduced-DOF snake may be defined as

$$\bar{U}_k = P\left(A_{\text{ref}} - A\right) + D\left(\dot{A}_{\text{ref}} - \dot{A}\right) \tag{25}$$

where A_{ref} and A are given by (24) and (22), respectively, and P and D are gains. Constraining the sum of the link lengths to be constant, the sums in (22) and (24) converge as m approaches infinity, so we can approximate A_{ref} by truncating the sum after the first term. Fig. 3 displays the steady state speed of a reduced-DOF snake with two benders of four links each, using the Angle-Sum Controller given by (21) and the simplified version of the Lateral Motion Controller given by (25), as the amplitude of the reference oscillatory motion (α or c_1) is varied, and with $\omega = 1$ Hz, $k_p = 1$, and $k_d = 0$. Steady state speed approaches a maximum for low amplitude oscillations, where drag forces approach their minimum. Both reduced-DOF snakes exhibit higher steady state speeds than a 3-link snake obeying (11), the corresponding full-DOF case.

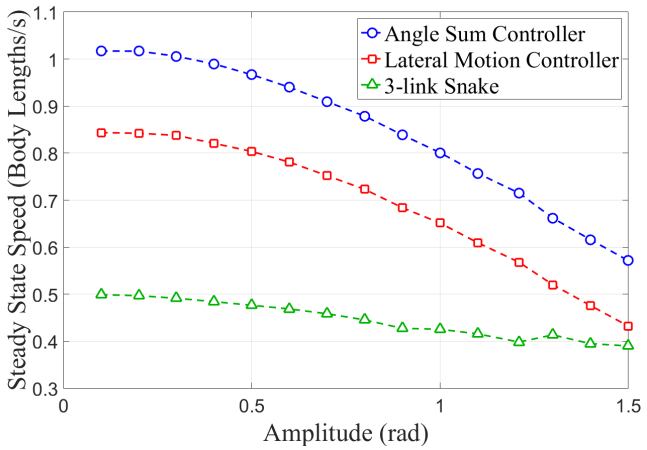

Fig. 3. Steady state speed vs. amplitude

B. Phase Offset Optimization

A reduced-DOF snake with N_b bending modules of N links each has the same number of DOFs as a full-DOF snake with (N_b+1) links, but a structure similar to a full-DOF snake with $N_b N$ links. We thus conjecture that the δ_{opt} that maximizes steady state speed in a reduced-DOF snake will fall between the optimal values for these two cases.

Fig. 4 displays δ_{opt} for full-DOF snake robots of various length, as c_n in Eq. (2) is varied, and where $c_t = 0$. The values of δ_{opt} for a reduced-DOF snake with equal link lengths, with $N_b = 2$ and $N = 4$, are also displayed, and as expected, remain between the corresponding values for the 3-link case and the 8-link case. Unlike the prediction given by (12), δ_{opt} depends on c_n in simulation. The results differ most sharply in the case of very low friction, where slipping is most pronounced. Note that the optimal phase offset is undefined for $c_n = 0$.

C. Joint Angle Optimization

The majority of previous work on snake robots has assumed that the snake's links are of identical length and mass. In a reduced-DOF snake, the actuation units may be longer and more massive than adjacent links, as in the design in Sec. II, so it is important to understand how unequal links affect locomotion. The body shape of a reduced-DOF snake moving according to (21) or (25) depends on the ratios of the joint angles in each bender module, which by (6) are constant throughout the entire bending motion. The joint angle ratios may thus be optimized to maximize steady state speed.

Fig. 5 displays steady state speed for a reduced-DOF snake robot with $N_b = 2$, $N = 4$, and fixed δ, as a function of bender geometry. Here, the middle two links are of constant length L and the outer two links lengths L_{out} are varied as some fraction of L, with mass and moment of inertia scaled according to link length. The steady state speed for each link length combination is a function of the ratio of the middle joint angle θ_{mid} to the outer two joint angles θ_{side}. As Fig. 5 shows, in the case of equal link lengths, steady state speed is maximized by setting $\theta_{\text{mid}} = \theta_{\text{side}}$. The optimal joint angle

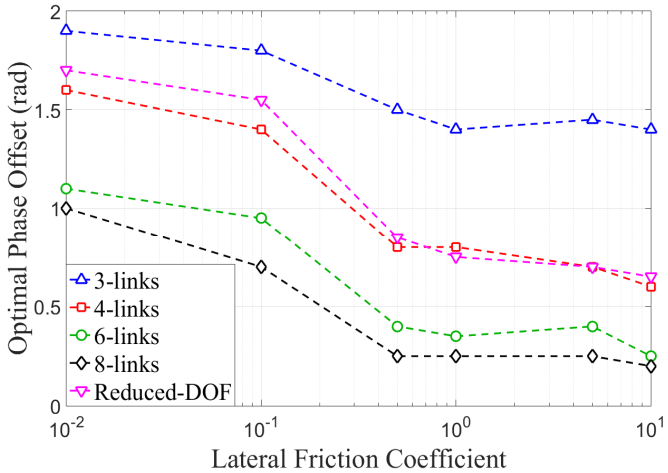

Fig. 4. Optimal phase-offset vs. lateral friction coefficient

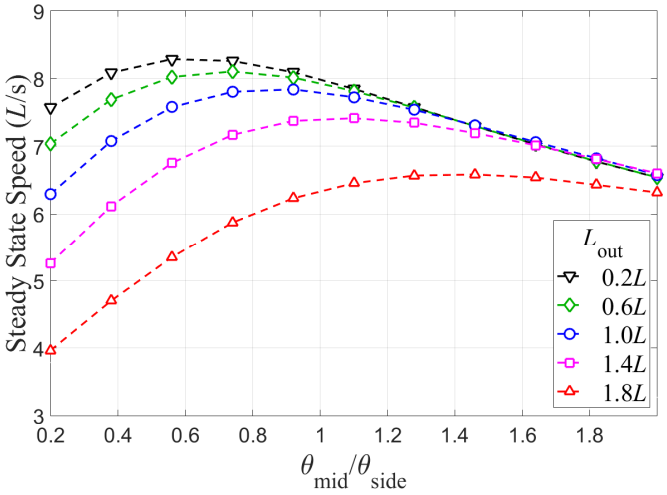

Fig. 5. Steady state speed vs. joint angle ratio

ratio grows with increasing outer link length, so that the longer links remain parallel to the direction of motion for longer periods than the short links, and the drag force on the snake is minimized.

VI. Conclusion

This paper demonstrated the use of underactuated bending modules in a snake robot. A multibody dynamic model was used to simulate planar locomotion and waypoint guidance in a snake robot with two, single-DOF bending units, and compute optimal control and design parameters.

Future work will include further investigation of cable actuation, series elastic actuation, and experimental validation with a prototype. The addition of a modular unit that produces rotation out of the plane of bending should allow for a snake robot with as few as three degrees of freedom to achieve path following in three dimensions. A 3-DOF design will also allow for exploration of three-dimensional locomotion gaits similar to sidewinding.

References

[1] S. Hirose, "Biologically Inspired Robots (Snake-like Locomotors and Manipulators)," *Oxford Univ. Press*, 1993.

[2] S. Ma, "Analysis of snake movement forms for realization of snake-like robots," *Robot. Autom. Proceedings. IEEE Int. Conf.*, vol. 4, pp. 3007–3013, Detroit, MI, USA, 1999.

[3] F. L. Chernousko, "Snake-like locomotions of multilink mechanisms," *JVC/Journal Vib. Control*, vol. 9, no. 1–2, pp. 235–256, 2003.

[4] E. Rezapour and P. Liljebäck, "Path following control of a planar snake robot with an exponentially stabilizing joint control law," *IFAC Proc.*, vol. 8, pp. 28–35, 2013.

[5] P. Liljebäck, I. U. Haugstuen, and K. Y. Pettersen, "Experimental investigation of a path following controller for planar snake robots," *11th Int. Conf. Control. Autom. Robot. Vision, ICARCV,* pp. 2325–2332, Singapore, 2010.

[6] P. Liljebäck and K. Y. Pettersen, "Waypoint guidance control of snake robots," *Proc. - IEEE Int. Conf. Robot. Autom.*, no. 7491, pp. 937–944, Shanghai, China, 2011.

[7] P. Liljebäck, K. Y. Pettersen, and Ø. Stavdahl, "Modelling and control of obstacle-aided snake robot locomotion based on jam resolution," *Proc. - IEEE Int. Conf. Robot. Autom.*, no. 7491, pp. 3807–3814, Kobe, Japan, 2009.

[8] P. Liljebäck, K. Y. Pettersen, Ø. Stavdahl, and J. T. Gravdahl, "Fundamental properties of snake robot locomotion," *IEEE/RSJ Int. Conf. Intell. Robot. Syst. IROS - Conf. Proc.*, pp. 2876–2883, Taipei, Taiwan, 2010.

[9] S. Hirose and H. Yamada, "Snake-like robots: Machine design of biologically inspired robots," *IEEE Robot. Autom. Mag.*, vol. 16, no. 1, pp. 88–98, 2009.

[10] D. Rollinson, "Control and Design of Snake Robots," *Doctoral Dissertation*, Dept. of Comp. Sci., Carnegie Mellon University, Pittsburg PA, June, 2014.

[11] D. Rollinson *et al.*, "Design and architecture of a series elastic snake robot," *IEEE/RSJ Int. Conf. Intell. Robot. Syst. IROS*, pp. 4630–4636, Chicago, IL, USA, 2014.

[12] A. A. Transeth, K. Y. Pettersen, and P. Liljebäck, "A survey on snake robot modeling and locomotion," *Robotica*, vol. 27, pp. 999, Castelo Branco, Portugal, 2009.

[13] W. S. Rone and P. Ben-Tzvi, "Static modeling of a multi-segment serpentine robotic tail," *ASME Int. Des. Eng. Tech. Conf. Comput. Inf. Eng. Conf.*, Boston, MA, USA, 2015.

[14] W. Saab, A. Kumar, and P. Ben-Tzvi, "Design and Analysis of a Miniature Modular Inchworm Robot," *ASME Int. Des. Eng. Tech. Conf. Comput. Inf. Eng. Conf.*, DETC2016-59386, Charlotte, NC, USA, 2016.

[15] W. S. Rone and P. Ben-Tzvi, "Continuum robot dynamics utilizing the principle of virtual power," *IEEE Trans. Robot.*, vol. 30, no. 1, pp. 275–287, Buffalo, NY, USA, 2014.

[16] W. S. Rone and P. Ben-Tzvi, "Continuum Robotic Tail Loading Analysis for Mobile Robot Stabilization and Maneuvering," *ASME Int. Des. Eng. Tech. Conf. Comput. Inf. Eng. Conf.*, Buffalo, NY, USA, 2014.

[17] W. S. Rone and P. Ben-Tzvi, "Mechanics Modeling of Multisegment Rod-Driven Continuum Robots," *J. Mech. Robot.*, vol. 6, no. 4, p. 41006, 2014.

[18] W. S. Rone and P. Ben-Tzvi, "Multi-segment continuum robot shape estimation using passive cable displacement," *ROSE - IEEE Int. Symp. Robot. Sensors Environ. Proc.*, no. 1334227, pp. 37–42, 2013.

[19] W. S. Rone and P. Ben-Tzvi, "Continuum Manipulator Statics Based on the Principle of Virtual Work," *ASME Int. Mech. Eng. Congr. Expo.*, Houston, TX, USA, 2012.

[20] W. Saab and P. Ben-Tzvi, "Design and Analysis of a Discrete Modular Serpentine Robotic Tail for Improved Performance of Mobile Robots," *ASME Int. Des. Eng. Tech. Conf. Comput. Inf. Eng. Conf.*, Charlotte, NC, USA, 2016.

[21] P. Racioppo, W. Saab, and P. Ben-Tzvi, "Design and Analysis of a Reduced Degree of Freedom Snake Robot," *ASME Int. Des. Eng. Tech. Conf. Comput. Inf. Eng. Conf.*, DETC2017-67377, Cleveland, OH, 2017.

[22] E. Haug, "*Computer-Aided Kinematics and Dynamics of Mechanical Systems, Volume I: Basic Methods*," Massachusetts: Allyn and Bacon, 1989.

[23] E. J. Haug and J. S. Arora, *Applied Optimal Design*. New York: Wiley Interscience, 1979.

[24] P. Liljebäck, K. Y. Pettersen, Ø. Stavdahl, and J. T. Gravdahl, *Snake Robots: Modeling, Mechatronics, and Control.* Springer-Verlag, London, 2013.